Structure of ^{32}P at high spins

R. Chakrabarti,[1,*] S. Mukhopadhyay,[1,†] R. Bhattacharjee,[1] S. S. Ghugre,[1] A. K. Sinha,[1] A. Dhal,[2] L. Chaturvedi,[3] M. Kumar Raju,[4] N. Madhavan,[2] R. P. Singh,[2] S. Muralithar,[2] B. K. Yogi,[5] and U. Garg[6]

[1]*UGC-DAE Consortium for Scientific Research, Kolkata Centre, Kolkata 700098, India*

[2]*Inter University Accelerator Centre, Aruna Asaf Ali Marg, New Delhi 110067, India*

[3]*Guru Ghasidas University, Bilaspur 495009, India*

[4]*Nuclear Physics Department, Andhra University, Visakhapatnam 530003, India*

[5]*Department of Physics, Government College, Kota 324009, India*

[6]*Department of Physics, University of Notre Dame, Notre Dame, Indiana 46556, USA*

(Received 1 September 2011; revised manuscript received 19 October 2011; published 29 November 2011)

Excited states in ^{32}P have been investigated up to high spins using γ-ray spectroscopic techniques following the ^{18}O(^{16}O, np)^{32}P fusion-evaporation reaction. Sixteen new transitions have been observed, and the level scheme has been extended up to $E_x = 9.637$ MeV. The multiclover Indian National Gamma Array (INGA) facilitated angular correlation and linear polarization measurements for spin-parity assignments. Branching ratios have been determined. The level scheme is indicative of excitation of nucleons across the sd-fp shell gap. The experimental observables were successfully interpreted by large-basis cross shell model calculations without resorting to any reduction of the single-particle energies of the $f_{7/2}$ and $p_{3/2}$ orbitals. These results suggest that any lowering of single-particle energies may not be required if an appropriate choice of valence space and effective interaction is made.

DOI: 10.1103/PhysRevC.84.054325 PACS number(s): 23.20.Lv, 23.20.En, 21.60.Cs, 27.30.+t

I. INTRODUCTION

The spectroscopic study of nuclei near the "island of inversion" provides understanding of the evolving shell structure in this region. Complete experimental information, viz. level energies, lifetimes, branching ratios, mixing ratios, spins, and parities, permits a critical test of the existing theoretical concepts related to the role of $T = 0$, $T = 1$ residual interactions with increasing neutron excess. Intruder configurations dominate the ground states of nuclei at the island of inversion. Shell-model calculations with *sdpf* interaction explain this inverted behavior of the ground states with strong excitations of two particles into intruder orbitals. Monte Carlo shell model (MCSM) calculations have given an impetus to the study of this region with a significantly better coverage of the model space, permitting more accurate incorporation of the increasing role of $T = 1$ residual interactions. They provide a better agreement with experimental data in the region of states with intruder contributions [1]. The MCSM reveals that the intruder contribution to the ground state is enhanced in a more gradual fashion across the boundaries of the island of inversion as compared to the predictions of the earlier shell-model calculations.

Nuclei with Z near the bottom of the *sd* shell and N near the top of the shell (which is likely to be influenced easily by the occupation of intruder dominated configurations) belong to a highly transitional region of nuclear structure enabling a sensitive testing of the various shell-model calculations. The isotopes of phosphorus present a good case study of this transitional region. For such nuclei, conventional shell-model calculations appear to be only partly successful in explaining their structure, and a consistent theory is yet to be developed as we have found in our earlier investigations on the structure of the ^{34}P nucleus [2]. The excitation energies of the low-lying positive-parity and negative parity states in ^{34}P were successfully reproduced with the spherical shell-model code Nushell@MSU [3] without having to take recourse to the lowering of the single-particle energies, as reported for odd-odd P nuclei in this region in Refs. [4,5]. However, computational limitations allowed only one particle to be excited to the *fp* shell. The calculations were unable to predict the transition probabilities and mixing ratios for the 1876-keV transition de-exciting the 2305-keV level, the second excited state of ^{34}P [2].

We present here the results of our study of ^{32}P ($N = 17$) nucleus, which has a similar structure as ^{34}P, and compare it with ^{30,34}P. The present work utilizes heavy-ion fusion evaporation reaction, which allowed us to investigate yrast states in ^{32}P up to high spins. Experimental data on the level structure of ^{32}P is mostly available from ^{29}Si(α, $p\gamma$)^{32}P [6–8], ^{30}Si(α, d)^{32}P [9], ^{31}P ($\vec{d}$, p) [10], and ^{2}H(^{31}P, $p\gamma$)^{32}P [11] reactions, thermal neutron capture studies (see, for example, Refs. [12–15]), and polarized thermal neutron capture studies [16]. The only previously reported heavy-ion investigation, by Baumann *et al.* [17], employed the ^{18}O + ^{16}O fusion-evaporation reaction. Yrast states were known up to $J^\pi = 5^-$. In the present work, the yrast states up to $J^\pi = (8^-)$ have been identified. Detailed spectroscopic analysis has been carried out from γ^n matrices to get the excitation energies and to build up the level scheme after assignment of spin and parity from angular correlation and linear polarization measurements. The present results have been compared with earlier reported values. Finally, shell-model calculation results are reported

*ritwika_c@delta.iuc.res.in

†Present address: Nuclear Physics Division, Bhabha Atomic Research Centre, Mumbai 400085, India.

for ^{32}P and compared with those of ^{30,34}P and earlier works on ^{32}P.

II. EXPERIMENTAL DETAILS

The ^{32}P nucleus was populated using the ^{18}O(^{16}O, np)^{32}P reaction. The ^{16}O beam at an incident energy of 34 MeV was delivered by the 15UD Pelletron at the Inter University Accelerator Centre (IUAC), New Delhi. The de-exciting γ rays were detected by the Indian National Gamma Array (INGA) [18] comprised of 18 Compton-suppressed Clover detectors. Three of these detectors were placed at $\theta \sim 32^\circ$ and at $\phi \sim 0^\circ$, $\sim 90^\circ$, and $\sim 180^\circ$, four were at $\theta \sim 57^\circ$ and at $\phi \sim 45^\circ$, $\sim 135^\circ$, $\sim 225^\circ$, and $\sim 315^\circ$, five were at $\theta \sim 90^\circ$ and at $\phi \sim 45^\circ$, $\sim 135^\circ$, $\sim 180^\circ$, $\sim 225^\circ$, and $\sim 315^\circ$, three were at $\theta \sim 123^\circ$ and at $\phi \sim 45^\circ$, $\sim 225^\circ$, and $\sim 315^\circ$ and three were at $\theta \sim 148^\circ$ and at $\phi \sim 0^\circ$, $\sim 90^\circ$, and $\sim 180^\circ$ with respect to the beam direction. The neutron-rich ^{18}O target was prepared by heating a 50-mg/cm^2-thick Ta foil in an atmosphere of enriched oxygen to form Ta_2O_5. The ^{18}O equivalent thickness was estimated to be $\sim$1.6 mg/cm^2 on each side. The target to detector distance was $\sim$24 cm. A logical OR condition of two- and threefold coincidences provided the trigger condition, and about a billion E_γ^N ($N \geqslant 2$) coincidences were recorded. The data collected using the CAMAC based multiparameter data acquisition system CANDLE [19] were written in list mode format for offline analysis.

III. DATA ANALYSIS AND RESULTS

The data were presorted to correct for any online drifts to ensure that there were relatively no gain changes between any two list mode data sets during the experiment, and were precisely gain matched to ensure that the data from each detector had a constant energy dispersion. A multifunctional, iterative energy calibration was performed using the standard radioactive sources ^{152}Eu, ^{133}Ba, and ^{60}Co along with the beam-off radioactivity data. The data were then sorted into symmetric γ-γ matrix and three-dimensional γ-γ-γ cube. All the symmetric and asymmetric matrices were constructed using our in-house data sorting code and RADWARE software package [20,21]. The drift correction and subsequent data analysis were done using the IUCSORT [22–24] and RADWARE [20,21] software packages, respectively.

The detection efficiency of the clover detectors was determined up to 1408 keV using the standard ^{152}Eu source. At higher energies, the efficiency was obtained following an extrapolation to the data from Refs. [25–28] (which was acquired using an identical setup).

A. Level scheme of ^{32}P

The projection spectrum of the symmetric γ-γ matrix is shown in Fig. 1. The major populated nuclei were ^{30,31,32}P, ^{29}Si, and ^{26}Mg. The peaks of ^{41}Ca, ^{41}K, ^{38}Ar, and ^{35}Cl, marked as contaminants ("C"), originate from the reaction of the ^{16}O beam with ^{27}Al in the target frame.

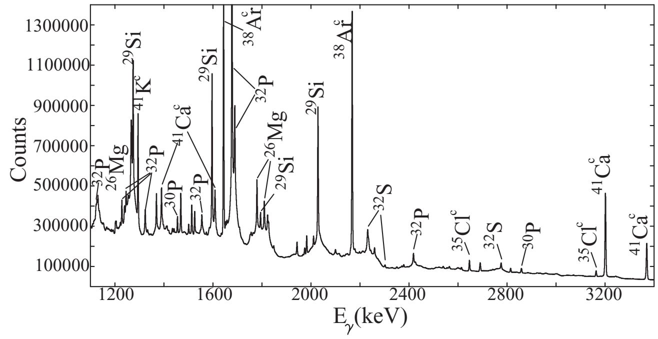

FIG. 1. Projection spectrum from ^{16}O+^{18}O fusion reaction at an incident beam energy of 34 MeV. "C" denotes contaminants.

Figure 2 depicts a background subtracted coincidence spectrum obtained by setting a gate on the 1689-keV ($4_1^- \rightarrow 3_1^+$) transition belonging to ^{32}P on one axis of the γ-γ matrix. Several new transitions are observed.

Figure 3 depicts a double-gated γ-ray spectrum from the cube with the gate on the 1677-keV ($3_1^+ \rightarrow 2_1^+$) and 1689-keV ($4_1^- \rightarrow 3_1^+$) transitions in ^{32}P.

The level scheme of ^{32}P was constructed from the symmetric matrices by studying the coincidence relationship among the de-exciting γ rays and was substantially extended to high spins with the addition of 16 new transitions (Fig. 4).

We have observed new yrast states at 5862 and 7417 keV. The observation of the 2418- and 1555-keV transitions de-exciting the above levels, as well as the 2220-keV transition, has helped to extend the level scheme up to an excitation energy of $\sim$9.6 MeV. Eckle *et al.* [10] had reported a level at 5860 keV, which was tentatively assigned $J^\pi = 2^-$. The observation of several parallel decay paths connecting levels of established spin and parity with the newly observed levels along with the angular correlation and polarization measurements of the new transitions, 2418 and 381 keV (Sec. III B) have led us to the assignment of $J^\pi = 6^{(-)}$, $J^\pi = 5^{(-)}$ to the 5862- and 5481-keV levels, respectively.

The 7417-keV level was observed to be connected to the 5862-keV level by a path parallel to the 1555-keV transition via the 603- and 952-keV transitions. The 7417-keV level is also connected to the the already established 4698-keV level via the 603- and 2116-keV transitions. Similarly, the 5862-keV level

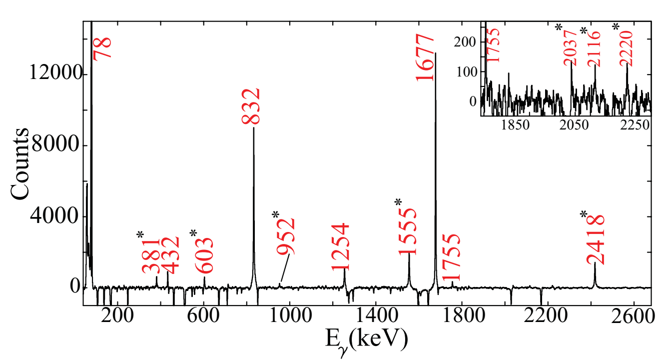

FIG. 2. (Color online) Coincidence spectrum with gate on 1689-keV transition in ^{32}P. The new assigned γ rays are marked with an asterisk.

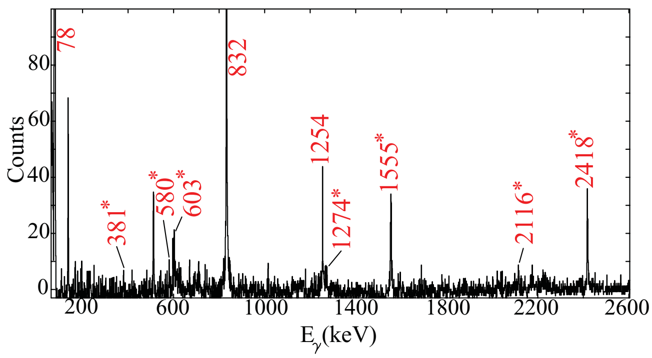

FIG. 3. (Color online) Coincidence spectrum with gate on 1677- and 1689-keV transitions in ^{32}P. The new assigned γ rays are marked with an asterisk.

was found to decay via parallel transitions of energy 1586 and 381 keV to the previously known 4276-keV ($J^\pi = 5^-$) level and the newly observed 5481-keV level, respectively. The 381- and 2037-keV transitions were placed in coincidence, and parallel to the 2418-keV transition, and connects the newly observed 5862-keV level to the known 3444-keV ($J^\pi = 4^-$) level.

Apart from the above-mentioned transitions, several other new transitions of energy 580, 623, 714, 955, 1274, 2139, 2559 keV were observed in the present study and placed in the level scheme. The excitation energies and the transitions energies are listed in Table I.

The presence of Doppler shapes in the low-lying intense transitions of the level scheme did not permit us to extract reliable information on the intensity of the observed transitions. However, the branching ratios of transitions (depopulating a particular level) were obtained from a symmetric γ-γ matrix, constructed with the data recorded in detectors placed at $\sim 90^\circ$ only, by top gating. This was done to avoid the Doppler shapes and shifts. The use of data at 90° was justified since the level sequence has mostly dipole transitions, and the experimental branching ratios obtained for known levels compare very well with the values reported previously. In Table II the branching ratios obtained in the present work are compared with the previously available value, as well as with the theoretical predictions (Sec. IV). The branching ratios for some transitions could not be determined since top gating was not feasible in those cases.

B. Determination of spin and parity

The conventional method of determination of the multipolarity of the observed transitions in $\gamma-\gamma$ spectroscopy is the DCO (directional correlations of the γ rays de-exciting oriented states) method described in Refs. [30–32]. This method is based on the observed coincidence intensity anisotropy, obtained from the angle dependent $\gamma-\gamma$ coincidences. The basic principle behind the distinction between dipole and quadrupole transitions is the fact that the angular distribution for a stretched dipole transition has a maximum at $\theta = 90^\circ$ and minimum at $\theta = 0^\circ$ or 180° and the reverse is true for a stretched E2 transition. However, having a detector at 0° or at 180° is not practically feasible. The angular distribution

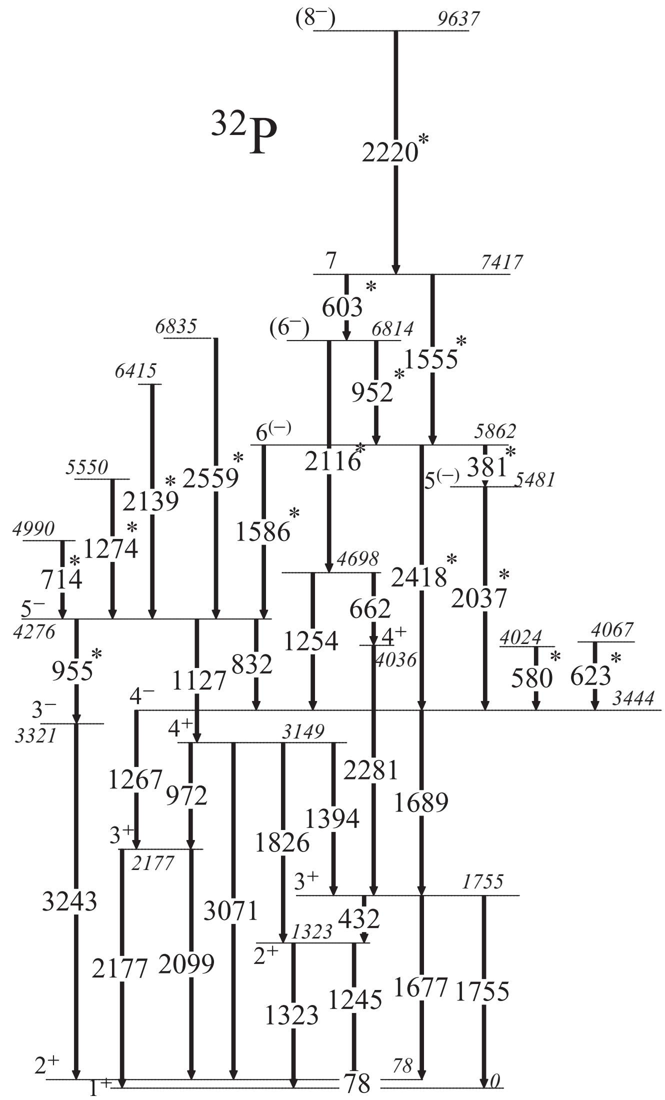

FIG. 4. Level scheme of ^{32}P. The new transitions are indicated by an asterisk.

measurements are usually performed in the singles mode, which has its own limitations, especially for weaker transitions of interest. Hence, coincidence intensity anisotropy measurements are used to obtain this information. Experimentally the coincidence anisotropy ratio is defined as

$$R_{\rm DCO} = \frac{I_{\gamma 1}\ (\text{at}\,\theta\ \text{gated by}\ \gamma_2\ \text{at}\ 90^\circ)}{I_{\gamma 1}\ (\text{at}\ 90^\circ\ \text{gated by}\ \gamma_2\ \text{at}\,\theta)}. \quad (1)$$

The present configuration of INGA has $\theta \sim 32^\circ$ or 148°. At these angles, appreciable Doppler shapes for fast transitions (de-exciting levels with $\tau_{\rm level} <$ stopping time of the recoil) are observed. The presence of fast transitions, viz. 1677 and 1689 keV at low spins in ^{32}P prohibits the application of this method. It is not possible to properly gate on γ rays with shapes at forward and backward angles since the gates would then be quite wide, and the limits are not precisely known. This would also result in a significant contribution from contaminants in the gated spectrum. Moreover, the line shapes of the neighboring 1677- and 1689-keV transitions

TABLE I. Transition energy, multipolarity of the γ rays, and the energy and spin assignments of the initial and final states in ^{32}P.

E_γ [a] (keV)	Multipole[b]	E_i [a] (keV)	E_f [a] (keV)	J_i^π	J_f^π
78.2	$(M1)$[c]	78	0	2_1^+	1_1^+
380.6	$M1$	5862	5481	$6_1^{(-)}$	$5_2^{(-)}$
432.4	$M1+E2$[c]	1755	1323	3_1^+	2_2^+
579.9		4024	3444		4_1^-
602.7		7417	6814	7_1	(6_2^-)
623.1		4067	3444		4_1^-
662.1		4698	4036		4_2^+
713.9		4990	4276		5_1^-
832.2	$M1$	4276	3444	5_1^-	4_1^-
951.7	$(M1)$[c]	6814	5862	(6_2^-)	$6_1^{(-)}$
955.1	$(E2)$	4276	3321	5_1^-	3_1^-
972.1	$M1+E2$	3149	2177	4_1^+	3_2^+
1126.5	$E1+M2$[c]	4276	3149	5_1^-	4_1^+
1245.1	$(M1)$[c]	1323	78	2_2^+	2_1^+
1254.2		4698	3444		4_1^-
1267.3	$E1+M2$[c]	3444	2177	4_1^-	3_1^+
1274.0		5550	4276		5_1^-
1323.1	D	1323	0	2_2^+	1_1^+
1394.4	$M1+E2$[c]	3149	1755	4_1^+	3_1^+
1554.9	$(E1+M2)$	7417	5862	7_1	$6_1^{(-)}$
1586.2	$(M1)$	5862	4276	$6_1^{(-)}$	5_1^-
1677.1	$M1$[c]	1755	78	3_1^+	2_1^+
1689.0	$E1$[c]	3444	1755	4_1^-	3_1^+
1755.1	$(E2+M3)$[c]	1755	0	3_1^+	1_1^+
1825.7	$(E2+M3)$[c]	3149	1323	4_1^+	2_2^+
2036.7	$(M1)$	5481	3444	$5_2^{(-)}$	4_1^-
2098.8	$M1+E2$[c]	2177	0	3_2^+	1_1^+
2115.8	$(E1)$	6814	4698	(6_2^-)	
2139.0		5583	3444		4_1^-
2177.4	$(E2+M3)$[c]	2177	0	3_2^+	1_1^+
2220.4		9637	7417	(8_1^-)	7_1
2281.0		4036	1755	4_2^+	3_1^+
2418.4	$E2+M3$	5862	3444	$6_1^{(-)}$	4_1^-
2558.8		6835	4276		5_1^-
3071.3	$(E2+M3)$[c]	3149	78	4_1^+	2_1^+
3242.5	$E1+M2$[c]	3321	78	3_1^-	2_1^+

[a]The quoted energies are within ±1 keV.
[b]Lowest multipolarity and dominant electromagnetic nature quoted for newly assigned transitions except for 2418- and 1555 keV, which appear evidently mixed (see text for details).
[c]From NNDC [29].

merge with each other so as to render gating on either of the transitions impossible.

These limitations can be circumvented if we were to define the anisotropy ratio as

$$R_{\text{anist}} = \frac{I_{\gamma 1} \text{ at } 32^\circ \text{ gated by } \gamma_2 \text{ at } 90^\circ}{I_{\gamma 1} \text{ at } 57^\circ \text{ gated by } \gamma_2 \text{ at } 90^\circ}. \tag{2}$$

Two asymmetric angle-dependent $\gamma-\gamma$ matrices were constructed, where the energies deposited in detectors at 90° were plotted along one axis, and along the other axis one of the matrices had coincidence events detected in detectors at 32° whereas the other matrix had coincidence events in

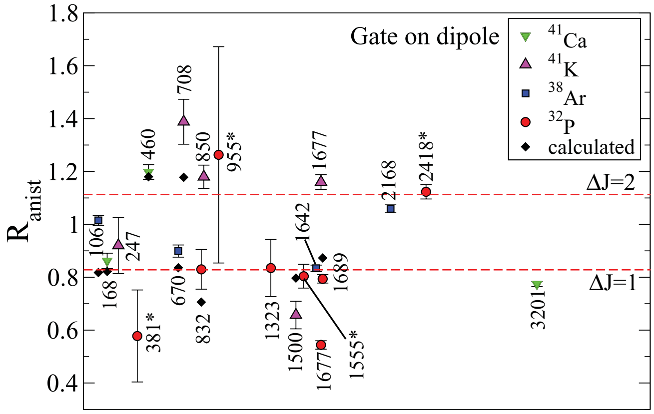

FIG. 5. (Color online) Plot of the experimental and calculated R_{anist} values for transitions in ^{41}Ca, ^{41}K, ^{38}Ar, and ^{32}P when the gate is on a dipole transition. The new transitions are indicated by an asterisk.

detectors at 57°. The advantage of this procedure is that the gates are always set on transitions at detectors placed at 90°, thus avoiding the line shapes. The intensity of the coincident γ ray (γ_1), whose multipolarity is to be extracted, was obtained first at 32° and then at 57°, and the ratio of these intensities (R_{anist}) was determined. Since the ratio of intensity of the same transition is observed, but in different detectors, the value of R_{anist} needs to be corrected for its dependence on the position of the detectors and the number of detectors at that particular position (angle). This was done by using the efficiency data of the 32° and 57° detectors. The experimental R_{anist} values were divided by the ratio of the counts obtained in the singles measurement with ^{152}Eu source in detectors at 32° and 57° detectors at corresponding energies. The plot of the experimental and calculated R_{anist} is given in Fig. 5.

Initially this ratio was determined for several strong transitions of known multipolarity in ^{41}Ca, ^{41}K, and ^{38}Ar [29] showing no line shape. As seen from Fig. 5, a clear distinction between quadrupole and dipole transitions is evident and the known multipolarities are reproduced. The weighted average of the experimental R_{anist} for dipole transitions was found to be ∼0.83 and that for quadrupole transitions was ∼1.11; lines corresponding to these values have been drawn to guide the eye. The conventional DCO measurement yielded a similar trend in the intensity anisotropy. Having established the validity of this procedure, the same was applied for the transitions in ^{32}P. The areas under the peaks for transitions having Doppler shape were computed from the corresponding gated spectra using the "LINESHAPE" code [33]. This program calculates line shape using the velocity profiles of the recoils (from Monte Carlo simulation) and the assumed values for the lifetimes of the observed transitions as well as those of the unobserved feeder transitions. From the proximity of the R_{anist} value to the $\Delta J = 1$ or the $\Delta J = 2$ line, it is possible to effectively distinguish between dipole and quadrupole transitions, respectively. An important point to be noted is that the anisotropy ratio, be it R_{DCO} or R_{anist}, is dependent on the multipolarity of the gating transition; the results in Fig. 5 have been obtained with gates on dipole transitions. Also, this ratio (Fig. 5) does not give the extent of mixing present, but provides

TABLE II. Comparison of experimental and theoretical branching ratios in ^{32}P.

E_x	J_i^π	J_f^π	E_γ	Experimental branching (%)		Theoretical branching (%)	
(keV)			(keV)	Earlier work[a]	Present work[b]	Theo. I	Theo. II
78	2_1^+	1_1^+	78		100		
1323	2_2^+	2_1^+	1245	40.6	47(1)	26.4	17.9
		1_1^+	1323	59.4(10)	53(1)	73.6	82.1
1755	3_1^+	2_2^+	432	2.0	1.4(1)	4.8	8.9
		2_1^+	1677	95.9(5)	97.6(1)	95.2	90.4
		1_1^+	1755	2.1(5)	1.1(1)	0.04	0.6
2177	3_2^+	2_1^+	2099	91.0	96.7(18)	86.6	85.9
		1_1^+	2177	9.0(9)	3.3(3)	13.4	14.1
3149	4_1^+	3_2^+	972	20.2(3)	25.4(9)	3.0	5.7
		3_1^+	1394	13.4(6)	13.9(6)	59.6	48.3
		2_2^+	1826	59.4(6)	55.6(14)	20.4	32.7
		2_1^+	3071	7.1(3)	5.1(4)	17.1	13.3
3321	3_1^-	2_1^+	3243	75(2)	100		
3444	4_1^-	3_2^+	1267	6.0(12)	1.8(3)		0.7
		3_1^+	1689	94.0(12)	98.3(25)		99.2
4276	5_1^-	4_1^-	832	77(12)			50.9
		3_1^-	955				1.0
		4_1^+	1127	23(12)			48.1
4036	4_2^+	3_1^+	2281		100		
4698		4_2^+	662	7.8(7)	15(2)		
		4_1^-	1254	82.6(17)	85(8)		
5481	$5_2^{(-)}$	4_1^-	2037		100		
5862	$6_1^{(-)}$	$5_2^{(-)}$	381		8.2(4)		0.2
		5_1^-	1586		2.6(2)		37.6
		4_1^-	2418		89.2(18)		62.2

[a]Reference [11].
[b]Errors quoted include fitting errors only.

a qualitative way of determining the *dominant* multipolarity. The calculated R_{anist} were determined for transitions with known multipolarities and mixing ratios using the code ANGCOR [34,35], and were found to agree reasonably with the experimental values (Fig. 5). The multipolarities extracted for known transitions in ^{32}P were found to be in agreement with the previous assignments. Among the new transitions, those with energies of 2418 and 955 keV were assigned as quadrupole transitions, whereas those with energies of 381 and 1555 keV were found to be dipole transitions.

Figure 6 is a plot of the calculated R_{anist} as a function of mixing ratio for a $J = 7 \rightarrow 6$ transition, with the area between the horizontal lines representing the uncertainty (statistical) in the experimental R_{anist} of the 1555-keV transition. A similar plot for the 2418-keV ($J = 6 \rightarrow 4$) transition is presented in Fig. 7. The physically acceptable region of overlap between the calculated and the observed R_{anist} provides a possible range of values for the mixing ratio. Since the R_{ainst} was obtained from the data at only two angles, this method of extracting mixing ratios has limited accuracy compared to the conventional method of angular distribution. Hence these measurements are only indicative of an almost pure, predominantly $\Delta J = 1$ and $\Delta J = 2$ nature for the 1555- and the 2418-keV transitions, respectively, with small admixtures of higher multipolarity. Limited statistics did not allow reliable angular correlation measurements for some of the new transitions.

The angular correlation measurement is not sensitive to the electric or magnetic nature of the radiation and polarization measurements are required for obtaining this information. The use of clover detectors facilitated such measurements

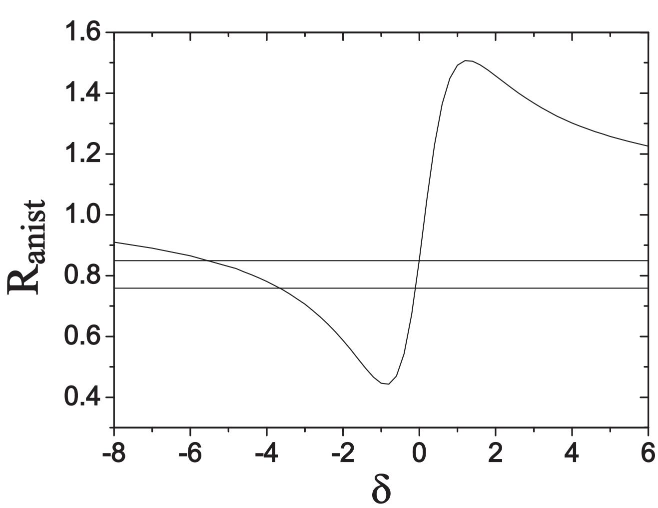

FIG. 6. Plot of the calculated R_{anist} as a function of mixing ratio for a $J = 7 \rightarrow 6$ transition. The area between the horizontal lines represent the uncertainty in the observed R_{anist} of the 1555-keV transition.

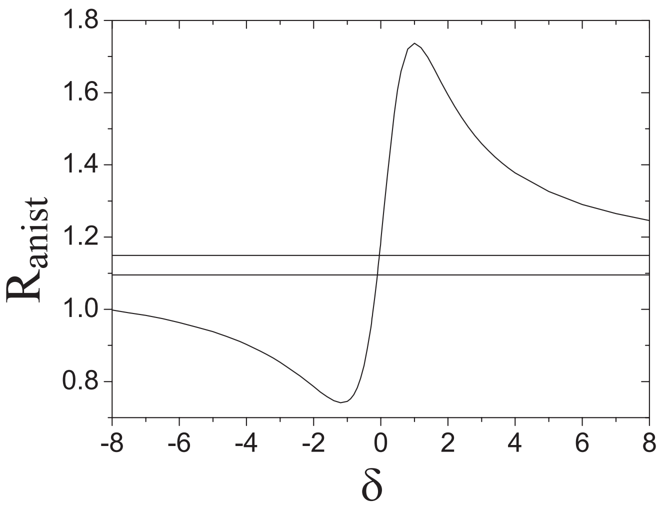

FIG. 7. Plot of the calculated R_{anist} as a function of mixing ratio for a $J = 6 \rightarrow 4$ transition. The area between the horizontal lines represent the uncertainty in the observed R_{anist} of the 2418-keV transition.

since the clover detector can act as a Compton polarimeter. Linear polarization measurements have been discussed in detail in our earlier work [2]. Experimentally we measure the asymmetry or Δ_{IPDCO} (IPDCO: integrated polarizational-directional correlation from oriented nuclei) defined as

$$\Delta_{\text{IPDCO}} = \frac{aN_{\perp} - N_{\parallel}}{aN_{\perp} + N_{\parallel}}, \tag{3}$$

where $N_{\perp}$ and $N_{\parallel}$ are the number of photons with a given energy scattered along the direction perpendicular and parallel to the reaction plane, respectively, in the detectors placed at $\sim 90^{\circ}$, and in coincidence with another photon detected in at least one other detector in the array. The asymmetry between the perpendicular and parallel scattering with respect to the reaction plane distinguishes between electric and magnetic transitions. "a" denotes the correction due to the asymmetry in the response of the clover segments. This factor is energy dependent ($a = a_0 + a_1 E_{\gamma}$), and is determined using a radioactive source (having no spin alignment) under similar conditions. This correction factor is defined as [36,37]

$$a = \frac{N_{\parallel}(\text{unpolarized})}{N_{\perp}(\text{unpolarized})}. \tag{4}$$

In the present work a_0 was found to be 0.9963(38) and a_1 was found to be $(-2.85 \pm 5.36) \times 10^{-6}$ keV^{-1}; a_1 being negligibly small was not considered in the calculations. Δ_{IPDCO} measurements required the construction of two asymmetric γ-γ matrices whose one axis corresponds to perpendicular or parallel scattered events in detectors placed at 90°, and the other axis corresponds to the total energy recorded in any of the other detectors. The gates were set on the latter axis, and the asymmetry (Δ_{IPDCO}) was obtained from the intensity of the coincident, scattered (perpendicular or parallel) γ rays, using Eq. (3). Figure 8 is a plot of the asymmetry values of several transitions of known electromagnetic nature in ^{41}Ca, ^{41}K, ^{38}Ar, and ^{32}P, as well as for some new transitions in ^{32}P. Detailed information is presented in Table III. At a given energy, a positive value indicates a dominantly electric transition, a negative value indicates a dominantly magnetic transition, whereas a near-zero value indicates a mixed transition. This analysis confirms the previously reported spins and parities of the levels in ^{41}Ca, ^{41}K, ^{38}Ar, and ^{32}P [29] and provides firm basis for new assignments in ^{32}P. Further, the calculated asymmetry

TABLE III. Experimental and calculated asymmetry (Δ_{IPDCO}) in ^{41}Ca, ^{41}K, ^{38}Ar, and ^{32}P.

E_{γ} (keV)	Mixing ratio (δ)[a,b]	Δ_{IPDCO} (experimental)	Δ_{IPDCO} (calculated)
	^{41}Ca		
460	0	0.147(8)	0.153
545	−0.01(3)	−0.065(15)	−0.078
3201	−0.02(1)	0.029(8)	0.006
	^{41}K		
708	0	0.123(34)	0.108
850	0	0.094(12)	0.105
1294	0.118(12)	−0.063(32)	−0.088
1468	0	0.079(24)	0.056
1500	−0.06(12)	0.053(27)	0.023
1513	0	0.041(32)	0.05
1677	0	0.052(13)	0.056
	^{38}Ar		
670	0.011(13)	−0.032(12)	−0.081
1642	0.016(13)	0.012(9)	0.034
2168	0	0.062(14)	0.049
	^{32}P		
381		−0.082(102)	
432	−0.12(10)	−0.055(87)	−0.083
832	−0.14(2)	−0.074(36)	−0.038
972	−0.11(4)	−0.052(74)	−0.040
1555		−0.012(74)	
1826	0.07(7)	0.031(30)	0.050
2418		0.037(63)	

[a]Reference [29].
[b]For transitions assigned $E2$ in NNDC, δ was considered zero if not reported.

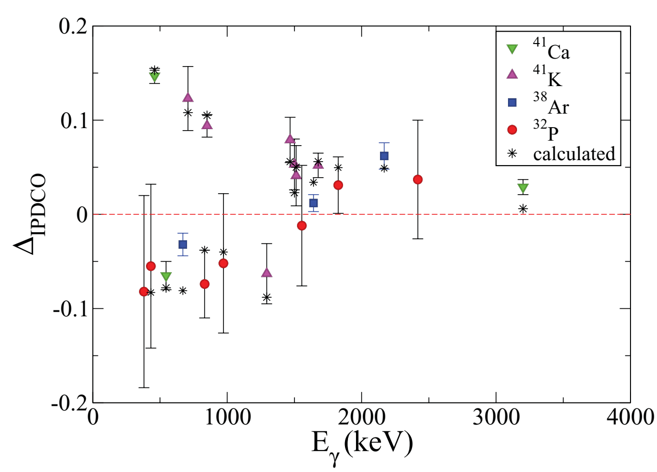

FIG. 8. (Color online) Plot of the experimental and calculated Δ_{IPDCO} as a function of γ-ray energy for transitions in ^{41}Ca, ^{41}K, ^{38}Ar, and ^{32}P (see Table III).

values for transitions with known mixing ratios were determined with $\sigma/J = 0.3$ using the procedure described in Ref. [2] and are also plotted in Fig. 8. The agreement between the experimental and calculated values is quite reasonable. The assigned spin-parities for ^{32}P are presented in Table I.

The R_{ainst} and Δ_{IPDCO} measurements for the 2418-keV transition (Figs. 5 and 8, and Table III) de-exciting the 5862-keV level indicate that this transition has a predominantly $E2$ nature with a small $M3$ admixture. Hence the 5862-keV level was assigned $J^\pi = 6^{(-)}$. The 381-keV transition, which connects the 5862-keV level (assigned $J^\pi = 6^{(-)}$) to the newly observed 5481-keV level, was found to be a dipole with a dominant magnetic nature. Hence the 5481-keV level should be $J^\pi = 5_2^-$, assuming stretched transitions. Under similar considerations it follows that the 2037-keV transition connecting the 5481-keV level to the already established 3444-keV ($J^\pi = 4^-$) level is of $M1$ nature. Similarly, considering the spin-parities of the 5862- and 4276-keV levels, the 1586-keV transition is proposed to be a magnetic dipole. The 9637-keV level is suggested to be 8^- on the basis of the theoretical predictions (Fig. 10). Similarly, the 6814-keV level is a likely candidate for 6_2^-, based on comparison with the theory. Of course, only the dominant multipolarity and electromagnetic nature could be determined for all these transitions.

1. 7417-keV level

The ^{30}Si(α, d) reaction by Vecchio *et al.* [9] had identified a level at $E_x = 7420 \pm 50$ keV in ^{32}P with a high (α, d) cross section. Angular distributions were obtained and DWBA analysis was carried out to determine the L transfers to this state. From this analysis the above state was tentatively assigned a $J^\pi = 7^+$ and believed to be arising out of $2\hbar\omega$ excitations with a fully aligned $(f_{7/2})^2$ configuration. The γ-ray spectroscopy following the fusion evaporation reaction between ^{18}O and ^{16}O identifies a level at $E_x \sim 7417$ keV (in present work) and at 7415 keV in Ref. [17]. Baumann *et al.* [17] have suggested it to be the same state as that observed by Vecchio *et al.* [9]. From the information available on the even-A phosphorus nuclei, a 2p-2h, $J^\pi = 7^+$, $(f_{7/2})^2$ state is expected in this energy domain. For example, in ^{34}P the 6236-keV level has been tentatively identified as a possible candidate for the above state [2,5]. Further, a similar state in ^{30}P was observed at $\sim$7231 keV [9,17]. In the present work, the experimental angular correlation measurement for the 1555-keV transition de-exciting the 7417-keV level in ^{32}P indicates a predominantly $\Delta J = 1$ nature. However, the uncertainties in the experimental Δ_{IPDCO} value for the 1555-keV transition did not allow us to conclusively assign an $E1 + M2$ or $M1 + E2$ nature to the transition (Table III) (Fig. 8). Hence a $J^\pi = 7^+$, 7^-, 6^+, or 6^- assignment is possible for this level. Considering the theoretical two-body matrix elements and the experimental γ-ray energies (1555 and 603 keV, respectively) connecting the 7417-keV level ($J^\pi = 7^+$, 7^-, or 6^+) to the $J^\pi = 6_1^-$ and 6_2^- state, the reduced transition probabilities, branching ratios, and lifetimes were calculated, and are presented in Table IV. We have not considered a $J^\pi = 6^-$ assignment to the 7417-keV level since

TABLE IV. The theoretical and experimental electromagnetic observables for the decay of the 7417- and 4698-keV levels in ^{32}P considering the various possible spin-parity assignments to these levels.

E_x (keV)	J_i^π	J_f^π	E_γ (keV)	Reduced transition probability (W.u.)		Branching ratio (%)		Lifetime (ps)
Expt.			Expt.	Theor.[a]		Expt.	Theor.[a]	Theor.[a]
7417	7_1^-							0.3
				$B(M1)$	$B(E2)$			
		6_1^-	1555	0.0240	0.7491	83.3(63)	96.2	
		6_2^-	603	0.0164	0.5836	16.7(22)	3.8	
7417	$7^+_{1(sd)}$							125.7
				$B(E1)$	$B(M2)$			
		6_1^-	1555	2.0×10^{-06}	0.0011	83.3(63)	95.3	
		6_2^-	603	0.0240	0.7491	16.7(22)	4.7	
7417	$6^+_{1(sd)}$							87.2
				$B(E1)$	$B(M2)$			
		6_1^-	1555	1.2×10^{-08}	2.5×10^{-04}	83.3(63)	4.3	
		6_2^-	603	5.0×10^{-05}	2.4×10^{-05}	16.7(22)	87.2	
4698	$5^+_{1(sd)}$							1.4
				$B(E1)$	$B(M2)$			
		4_1^-	1254	2.6×10^{-06}	0.0014	85(8)	0.7	
				$B(M1)$	$B(E2)$			
		4_2^+	662	0.0793	0.0006	15(2)	99.3	
4698	4_2^-							0.4
				$B(M1)$	$B(E2)$			
		4_1^-	1254	0.0453	2.1441	85(8)	99.8	
				$B(E1)$	$B(M2)$			
		4_2^+	662	1.9×10^{-05}	0.0334	15(2)	0.2	

[a]From Theo. II. See Sec. IV for details.

it would correspond to the third excited 6^- state, which is unlikely to be strongly populated. A $J^\pi = 7^+$ assignment could originate either from a $0\hbar\omega$ (sd) or a $2\hbar\omega$ ($sdfp$) excitation. A pure sd 7^+ is predicted at an excitation energy 8.8 MeV ($E_{\text{theory}} - E_{\text{expt}} \sim 1.4$ MeV) (Theo. I in Fig. 10). The calculated lifetime in this case is ∼126 ps (Table IV). The 1555-keV transition de-exciting the 7417-keV level exhibits clear Doppler shape, which contradicts the possibility of such a long lifetime for this level, thus ruling out a pure sd 7^+ configuration for this state. A $2\hbar\omega$ excitation could give rise to a 7^+ state in this energy domain as mentioned earlier. These configurations could not be included in our present shell-model calculations due to computational limitations, rendering it impossible to comment either way on a 2p-2h 7^+ assignment. Interestingly, the calculations are supportive of a 7^- assignment since the predicted excitation energy, branching ratio, and lifetime are in good agreement with experimental observations (Table IV) (Fig. 10). A pure sd 6^+ assignment was also found to be unlikely. Although the predicted energy of the pure sd 6^+ state (7392 keV) is quite close to the 7417-keV level (Fig. 10), the theoretically predicted branching ratio and lifetime rule out such an assignment (Table IV). Thus the 7417-keV level is either $J^\pi = 7^+$ or 7^- and it is not possible to unambiguously resolve between these two options.

2. 4698-keV level

From the present data, we were unable to arrive at an unambiguous assignment of spin and parity for the observed 4698-keV level. There were Doppler broadening related difficulties in obtaining the experimental angular correlation and polarization values. Earlier reports have suggested $J^\pi = 3^+$, 5^+, or 4^- for this level [10]. If this level is $J^\pi = 3^+$, it would be a highly non-yrast state (the third excited 3^+), which is unlikely to be observed in a heavy-ion-induced reaction. Theoretically predicted excitation energy of $J^\pi = 3^+$ (2.916 MeV) is also in disagreement with such an assignment (Fig. 10). Branching ratios calculated with the 4698-keV level as a pure sd 5^+ state (predicted at 4.976 MeV) completely disagree with the experimental values (Table IV). This would imply that if this level has $J^\pi = 5^+$, it should have a significant contribution from $2\hbar\omega$ excitations and hence would then be the lowest intruder, yrast, positive-parity state. Computational limitations (Sec. IV) did not allow us to calculate the excitation energy of such a level. If we assume a $J^\pi = 4^-$ for this level, the predicted 5286-keV level (Fig. 10) would be its theoretical counterpart, which is 558 keV off the experimental value. The predicted branching ratios in this case are in reasonable agreement with the observed values (Table IV). We note in passing that the deduced level scheme is characteristic of a single-particle/spherical structure devoid of deformed band structure.

IV. THEORETICAL CALCULATIONS

Nuclei in and around the island of inversion have been the playground for testing various theoretical nuclear models. Monte Carlo shell-model calculation (MCSM) [38] based on quantum Monte Carlo diagonalization with certain modifications in the two-body matrix elements (TBME) has been successfully used to explain the structure of nuclei in and around the island of inversion [1]. Utsuno *et al.* [1] have shown this model to work successfully for $N \sim 20$ unstable even-even isotopes of O, Ne, Mg, and Si. This model has also been applied in several works recently, viz. for ^{30}Mg [39], ^{28,29,30}Na [40–43], ^{27,29,31}Mg [44]. This approach in certain cases met with limited success, for example in ^{30}Mg [39].

Isotopes of P are *sd*-*pf* nuclei, which provide a unique opportunity for further investigation of this region. The structure of odd-A isotopes of P, like ^{31,35}P, have been explained using the MCSM formalism. Ionescu-Bujor *et al.* [45] in their work on ^{31}P found that the excitation energies were reproduced well (within 600 keV) by the MCSM calculations but there were some marked discrepancies in the prediction of the reduced transition probabilities. These findings led them to suggest that the *sd*-*pf* shell gap predicted by the SDPF-M interaction (5.3 MeV) for P isotopes with $N = 20$ may be too large, and that a more refined interaction and a wider model space was necessary to explain the high spin states in ^{31}P. In ^{35}P [46] the MCSM calculations using SDPF-M interaction successfully predicted the excitation energies. However, no comparison of experimental transition probabilities with theoretical predictions were carried out. The states of ^{35}P were also calculated using WBP interaction. But in this case the *sd*-*pf* shell gap had to be reduced by 1.2 MeV to obtain a good agreement between the predicted and observed values.

MCSM calculations have not been reported for even-A isotopes of P. Shell-model calculations with the Continuum Shell model code [47] were carried out for ^{32,34,36}P ($N = 17$, 19, 21, respectively) by Bender *et al.* [5] using the WBP [48] interaction. Ray *et al.* [4] have reported shell-model calculations for ^{30}P ($N = 15$) using the WBMB interaction [49]. In all these cases, the theoretical and experimental energies matched only after an *ad hoc* reduction in the single-particle energies of the $1f_{7/2}$ and $1p_{3/2}$ orbitals. We had reported our shell-model calculations for ^{34}P [2] using the code Nushell@MSU [3] in the *sd*-*pf* model space outside ^{16}O core with the WBMB interaction [49]. One $\hbar\omega$ calculation without any truncations in the sd shell could reproduce the negative-parity states [2] fairly well, without any lowering of the single-particle energies (SPEs), as was required in a similar calculation by Bender *et al.* [5] using the WBP interaction. The number of configurations possible in ^{30,32}P is enhanced as compared to that for ^{34}P and the resulting matrix dimensions are larger, necessitating some truncation in the sd shell space for generating the negative-parity states. Ray *et al.* [4], in their calculations for ^{30}P including an excitation of maximum two particles from $1d_{5/2}$ orbital, lowered the *sd*-*pf* shell gap by 4.5 MeV in order to reproduce the negative parity states. We have carried out similar truncated shell-model calculations for ^{30}P but without any lowering of the *sd*-*pf* shell gap. Figure 9 shows the difference between the experimental and the theoretical excitation energies of the first intruder state as a function of the number of particles excited from the $1d_{5/2}$ orbital in ^{30}P. The predicted excitation energy of negative-parity state approaches the experimental value with an increase in the $(d_{5/2})^{-n}$ excitations. The observed saturation in the difference may be due to the omission of configurations

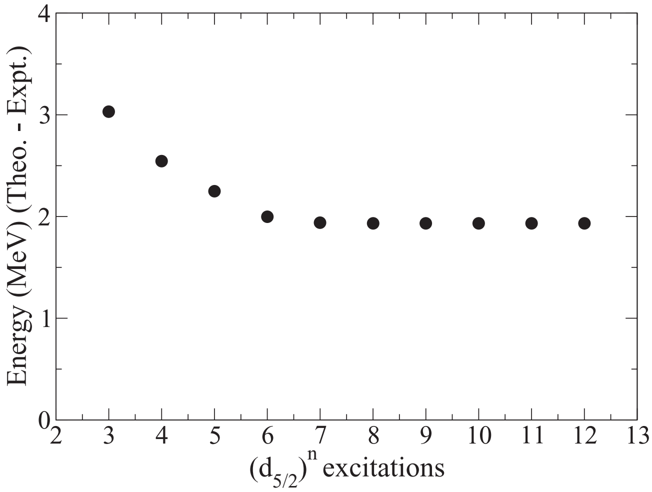

FIG. 9. Plot of the difference between experimental and shell-model predicted excitation energy of the first intruder state ($J^\pi = 2^-$) as a function of the number of particles (n) excited from $1d_{5/2}$ orbital in ^{30}P. The "*sdpfmw*" interaction has been used.

from inside the ^{16}O core. It has been established by Warburton *et al.* [49] that truncation of model space renders the ground state less bound, resulting in the predicted states occurring at higher excitation energies. The lowering of the excitation energy with increase in the configurations strongly suggests that the *ad hoc* lowering of the single-particle energy in previous works may not be realistic in the case of these nuclei.

We have carried out the shell-model calculations for ^{32}P without any reduction in SPE using the code Nushell@MSU [3] and the WBMB interaction [49]. The model space consisted of $d_{5/2}$, $s_{1/2}$, $d_{3/2}$, $f_{7/2}$, $p_{3/2}$, $p_{1/2}$ orbitals outside the ^{16}O core. For the low-lying positive-parity states, $0\hbar\omega$ calculations (labeled as Theo. I) carried out in the above model space using the *sdpfmw* interaction [49,50] resulted in a very good agreement with the observed excitation energies (Fig. 10). The predicted ground-state energy -175.576 MeV also matches very well with the experimental value of -175.65 MeV [51]. The negative-parity states were generated with a single particle excited to the fp shell along with some truncation in the sd shell.

Figure 11 shows the difference between experimental and theoretical excitation energies of the negative-parity states as a function of the number of particles excited from the $1d_{5/2}$ orbit. The $J^\pi = 4_2^-$ and 7^- assignments are tentative. Computational limitations dictated a minimum truncation allowing $n = 4$ particles to be excited from $1d_{5/2}$ orbital. Here again, we observe that, as in Fig. 9, the predicted excitation energy of negative-parity states approaches the experimental value with an increase in the $(d_{5/2})^{-n}$ excitations. The results for ^{32}P indicate that unlike ^{30}P (Fig. 9), most of the dominant configurations have been incorporated in the calculations as the difference approaches a near-zero value. The calculations on ^{30,32}P show that in this mass region, omission of important configurations is responsible for the excitation energies occurring at a higher value than their experimental counterparts and as these configurations

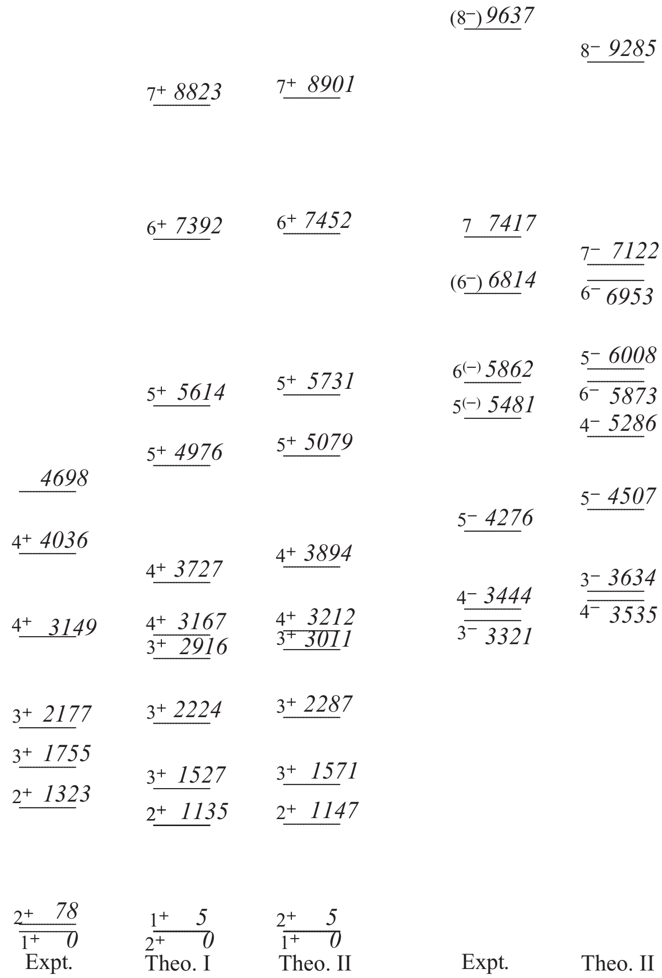

FIG. 10. Comparison between experimental and shell-model predicted levels in ^{32}P (see text for details).

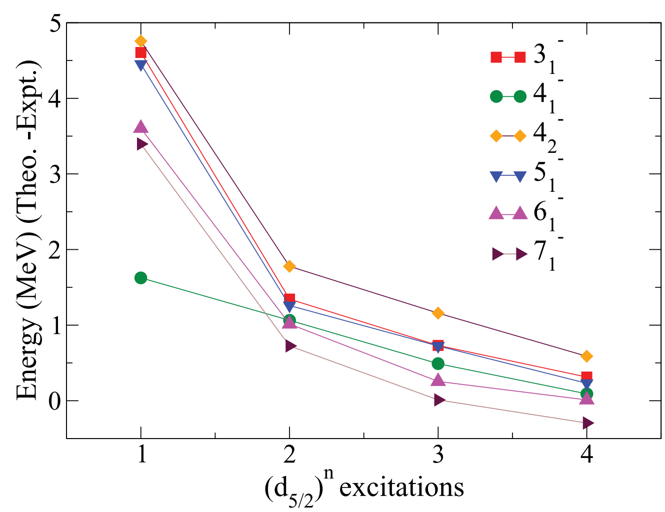

FIG. 11. (Color online) Plot of the difference between experimental and shell-model predicted excitation energy of negative-parity states as a function of the number of particles (n) excited from $1d_{5/2}$ orbital in ^{32}P. The "*sdpfmw*" interaction has been used (see text for details).

TABLE V. Average particle occupancies of negative parity states in ^{32}P from Theo. II.

J^π	E_x	$d_{5/2}$	$s_{1/2}$	$d_{3/2}$	$f_{7/2}$
3_1^-	3.634	10.901	2.322	1.769	1.000
3_2^-	5.086	10.811	1.903	2.286	1.000
4_1^-	3.535	10.934	2.409	1.657	1.000
4_2^-	5.286	10.724	1.891	2.384	1.000
5_1^-	4.507	10.820	1.792	2.389	1.000
5_2^-	6.008	10.548	2.578	1.874	1.000
6_1^-	5.873	10.872	2.110	2.018	1.000
6_2^-	6.953	10.343	2.262	2.395	1.000
6_3^-	7.402	10.406	2.334	2.260	1.000
7_1^-	7.122	10.798	1.569	2.634	1.000
7_2^-	8.255	10.227	2.232	2.541	1.000

get included, the predicted excitation energies approach the experimental values.

In view of our computational limitations, all the negative-parity states were generated with the minimum and maximum number of particle occupancies of $1d_{5/2}^{8-12}$, $1s_{1/2}^{0-4}$, $1d_{3/2}^{0-8}$, $1f_{7/2}^{0-1}$ (labeled as Theo. II). Figure 10 compares the negative-parity states with experiment. We can see that there is a notable agreement between the experiment and theory. To validate our truncation scheme, the positive-parity *sd*-shell states were also generated using the above truncations in the *sd* shell. As seen from Fig. 10, Theo. II compares well with the $0\hbar\omega$ calculations and the experimental values. The predicted ground-state energy -175.491 MeV is very close to the experimental value. The assignment of $J^\pi = 6^{(-)}$ to the observed level at $E_x = 5862$ keV and $J^\pi = 5_2^{(-)}$ to the level at $E_x = 5481$ keV is substantiated by the prediction of a 5873-keV ($J^\pi = 6^-$) (Theo. II) and a 6008-keV ($J^\pi = 5_2^-$) (Theo. II) level, respectively. The calculations predicted a closely lying 7^- state at 7122 keV (Theo. II) and 6^+ state at 7392 keV (Theo. I) and 7452 keV (Theo. II). The 7^+ state is predicted at 8823 keV in Theo. I and at 8901 keV in Theo. II. The possibility of the 7417-keV state having a pure *sd* 6^+ or a pure *sd* 7^+ configuration has already been ruled out in the earlier section. A $J^\pi = 7^-$ assignment is well supported by theory. The 9637-keV level was tentatively assigned $J^\pi = (8^-)$ as it appears to correspond to the predicted 9285-keV ($J^\pi = 8^-$) level. Similarly, the 6814-keV level may be 6_2^-, considering the predicted 6953-keV ($J^\pi = 6^-$) level. The average particle occupancies of the predicted negative-parity states in ^{32}P are listed in Table V.

The test of a nuclear model is how successfully it reproduces the excitation energies and the wave functions. The transition probabilities are highly sensitive to the composition of the wave functions and hence are suitable tests of the wave functions. In ^{34}P, the experimental mixing ratio of the 1876-keV transition connecting the lowest intruder state to the first excited state (2^+) could not be reproduced [2]. Bender *et al.* [5] have not considered mixing while calculating the transition probabilities in ^{34}P. The inability of present theoretical models to correctly predict the reduced transition probabilities in nuclei in the vicinity of the island of inversion in many cases has been discussed before.

In ^{32}P, the reduced transitions probabilities for transitions connecting positive parity states when calculated with and without truncations in the *sd* shell are given in Table VI, and a comparison with the experimental values is presented. The overall agreement is reasonably good. However, the predicted $B(E2)$ values for the 432-, 1755-, and 3071-keV transitions are not of the same order as the experimental values. The calculated $M1/E2$ and $E2/M3$ transition probabilities for transitions connecting the negative-parity states are given in Table VII. Among these, the reduced transition probabilities of only the 832-keV ($M1 + E2$) transition is known experimentally. The predicted values are in reasonable agreement with the experimental values in this case. Table VIII compares the experimental and theoretical transition probabilities of the $E1$ transitions in ^{32}P, using standard effective charges $e_p = 1.5$ and $e_n = 0.5$. The theoretical values are of the same order as the experimental values except for the $B(E1)$ value of

TABLE VI. Comparison of experimental and theoretical reduced $M1$, $E2$, and $M3$ transition probabilities for transitions between positive-parity states in ^{32}P.

E_x	J_i^π	E_γ	J_f^π	$B(M1)$ (W.u.)			$B(E2)$ (W.u.)			$B(M3)$ (W.u.)		
(keV)		(keV)		Expt.[a]	Theo. I	Theo. II	Expt.[a]	Theo. I	Theo. II	Expt.	Theo. I	Theo. II
78	2_1^+	78	1_1^+	0.166(8)	0.1632	0.1759		1.7928	1.7415			
1323	2_2^+	1245	2_1^+		0.001	$1.3E-04$		3.3371	3.2709			
	2_2^+	1323	1_1^+		0.004	0.0035		5.5459	5.2675			
1755	3_1^+	432	2_2^+	0.0117(11)	0.0238	0.0307	4.0(7)	0.0792	0.0785			
	3_1^+	1677	2_1^+	0.0060(7)	0.0018	0.0002	5.6(9)	11.3271	10.4356			
	3_1^+	1755	1_1^+				0.26(7)	0.0066	0.0744		1.0749	1.0147
2177	3_2^+	2099	2_1^+	0.048(9)	0.0452	0.0390	0.9(5)	0.5914	1.0273			
	3_2^+	2177	1_1^+				3.8(9)	6.1905	5.3619		0.7421	1.1035
3149	4_1^+	972	3_2^+	0.0133(15)	0.0098	0.0140	0.6(5)	0.9705	0.9219			
	4_1^+	1394	3_1^+		0.0313	0.0153	6.3(8)	10.2600	9.9104			
	4_1^+	1826	2_2^+				7.6(9)	7.0852	7.3305		0.1124	0.0824
	4_1^+	3071	2_1^+				0.068(8)	0.6396	0.3297		0.0755	0.0222
4036	4_2^+	2281	3_1^+		0.1693	0.1607		0.7306	0.8396			

[a]Reference [29].

TABLE VII. Comparison of experimental and theoretical reduced $M1$, $E2$, and $M3$ transition probabilities for transitions between negative-parity states in ^{32}P.

E_x (keV)	J_i^π	E_γ (keV)	J_f^π	$B(M1)$ (W.u.) Expt.[a]	$B(M1)$ (W.u.) Theo. II	$B(E2)$ (W.u.) Expt.[a]	$B(E2)$ (W.u.) Theo. II	$B(M3)$ (W.u.) Expt.	$B(M3)$ (W.u.) Theo. II
4276	5_1^-	832	4_1^-	0.054(9)	0.0283	6.5(21)	1.9221		
	5_1^-	955	3_1^-				4.5003		0.0016
5481	$5_2^{(-)}$	2037	4_1^-		0.0678		9.0819		
5862	$6_1^{(-)}$	381	$5_2^{(-)}$		0.1067		0.3234		
	$6_1^{(-)}$	1586	5_1^-		0.0185		0.2300		
	$6_1^{(-)}$	2418	4_1^-				4.7986		1.3099

[a]Reference [29].

the 3243-keV transition. The discrepancies and deviations observed in reduced transition probabilities are most likely the artifacts of truncation.

Computational limitations that arose due to large basis space and matrix dimension allowed for only one particle to be excited to the $1f_{7/2}$ orbital in case of ^{30}P and ^{32}P, and, only one particle excited to the *fp* shell in ^{34}P. The deviation of the predicted transition probabilities (Tables VI–VIII) and branching ratios (Table II) from the experimental values, where present, may be attributed at least partially to this limitation. The need for an extended basis space and/or an appropriate Hamiltonian within the *sd-pf* model space, which takes into account all the possible intra- as well as intershell interactions, was conjectured in Ref. [2], and is strongly indicated in the present work as well.

V. CONCLUSIONS

The use of ^{16}O + ^{18}O fusion evaporation reaction provided access to yrast and near yrast states in ^{32}P. Several new transitions belonging to ^{32}P have been identified and placed in the decay scheme, which was extended up to $E_x = 9637$ keV and $J^\pi = (8^-)$. Angular correlation and linear polarization measurements helped in determining the spin and parity of several observed levels. Corresponding theoretical values were calculated for transitions with known mixing ratios and were found to be consistent with the experimental values. The branching ratios were also determined experimentally. The negative-parity states are of interest as they originate from the excitation of nucleons across the major shell into opposite parity orbitals. The higher lying positive-parity states could also have similar configuration. The experimental observables (J^π, E_x, branching ratio) are compared with the prediction of the spherical shell-model calculation using the code Nushell@MSU with *sdpfmw* interaction outside ^{16}O core. The observed positive-parity states were successfully reproduced by $0\hbar\omega$ calculations, indicating that these states are predominantly pure *sd* states. Truncated shell-model calculations involving an excitation of $n = 4$ particles from $1d_{5/2}$ orbital using the above interaction predicted the negative-parity states reasonably well. With increase in number of particles excited from the $1d_{5/2}$ orbital, the predicted excitation energies of the negative parity states are observed to approach the experimental values indicating that these states have predominantly $1d_{5/2}^{-n} \otimes 1f_{7/2}^1$ configurations. The overall qualitative agreement between the calculations and the experimental observables, especially the excitation energies, indicates that all important configurations and two-body matrix elements have been incorporated in the calculations. The *ad hoc* lowering of the SPE of $f_{7/2}$ and $p_{3/2}$ in some of the earlier calculations is not required and such adjustments appear to have been an artifact primarily of the matrix elements used, which are optimized for $A \approx 10-22$ nuclei and the earlier interpretation that the reduction in the energy gap between the neutron Fermi surface and fp shell is manifested by the lowering of SPE, may not hold true. The calculations point to the urgent need for a global parametrization of the TBME, especially the cross-shell terms.

ACKNOWLEDGMENTS

The authors thank all the participants of the INGA collaboration for their help in setting up the facility at IUAC, New Delhi. We are thankful to J. P. Greene (Argonne National

TABLE VIII. Comparison of experimental and theoretical reduced $E1$ and $M2$ transition probabilities in ^{32}P.

E_x (keV)	J_i^π	E_γ (keV)	J_f^π	$B(E1)$ (W.u.) Expt.[a]	$B(E1)$ (W.u.) Theo. II	$B(M2)$ (W.u.) Expt.	$B(M2)$ (W.u.) Theo. II
3321	3_1^-	3243	2_1^+	$8.0 \times 10^{-05}(23)$	2.6×10^{-04}		0.1831
3444	4_1^-	1267	3_2^+	$7.6 \times 10^{-05}(22)$	2.1×10^{-05}		0.0263
	4_1^-	1689	3_1^+	$5.0 \times 10^{-04}(10)$	6.9×10^{-04}		0.0409
4276	5_1^-	1127	4_1^+	$2.0 \times 10^{-04}(4)$	3.5×10^{-04}		0.0370

[a]Reference [29].

Laboratory) for preparing the ^{18}O target. Thanks are due to Kausik Basu of UGC-DAE CSR, Kolkata Centre for his help during the experiment. The authors would also like to acknowledge the Pelletron staff at IUAC, New Delhi. R.C. would like to acknowledge the financial assistance in the form of a fellowship ("Senior Research Fellowship", CSIR Sanction No. 91838(37)/2010-EMRI) from the Council of Scientific and Industrial Research (CSIR), Government of India. This work has been supported in part by the Department of Science and Technology, Government of India (Grant No. IR/S2/PF-03/2003-III) and the U.S. National Science Foundation (Grants No. PHY07-58100 and No. PHY-1068192).

[1] Y. Utsuno, T. Otsuka, T. Mizusaki, and M. Honma, Phys. Rev. C **60**, 054315 (1999).
[2] R. Chakrabarti *et al.*, Phys. Rev. C **80**, 034326 (2009).
[3] B. A. Brown and W. D. M. Rae, MSU-NSCL Report, 2007.
[4] I. Ray *et al.*, Phys. Rev. C **76**, 034315 (2007).
[5] P. C. Bender *et al.*, Phys. Rev. C **80**, 014302 (2009).
[6] F. E. H. Van Eijkern, G. Van Middelkoop, J. Timmer, and J. A. V. Luijk, Nucl. Phys. A **210**, 38 (1973).
[7] F. E. H. Van Eijkern, G. Van Middelkoop, W. A. Sterrenburg, and A. F. C. Buijense, Nucl. Phys. A **260**, 124 (1976).
[8] N. J. Davis and J. M. Neslson, J. Phys. G **13**, 375 (1987).
[9] R. M. Del Vecchio, R. T. Kouzes, and R. Sherr, Nucl. Phys. A **265**, 220 (1976).
[10] F. J. Eckle, G. Eckle, F. Merz, H. J. Maier, H. Kader, and G. Graw, Nucl. Phys. A **501**, 413 (1989).
[11] A. Kangasmäki, P. Tikkanen, J. Keinonen, W. E. Ormand, and S. Raman, Phys. Rev. C **55**, 1697 (1997).
[12] G. Van Middelkoop, Nucl. Phys. A **97**, 209 (1967).
[13] G. Van Middelkoop and P. Spilling, Nucl. Phys. **72**, 1 (1965).
[14] T. J. Kennett, W. V. Prestwich, and J. S. Tsai, Phys. Rev. C **32**, 2148 (1985).
[15] S. Michaelsen, C. Winter, K. P. Lieb, B. Krusche, S. Robinson, and T. Von Egidy, Nucl. Phys. A **501**, 437 (1989).
[16] J. De Boer, K. Abrahamas, J. Kopecky, and P. M. Endt, Nucl. Phys. A **352**, 125 (1981).
[17] P. Baumann, A. M. Bergdolt, G. Bergdolt, R. M. Freeman, F. Haas, B. Heusch, A. Huck, and G. Walter, Fizika (Suppl.) **10**, 11 (1978).
[18] S. Muralithar *et al.*, Nucl. Instrum. Methods Phys. Res. A **622**, 281 (2010).
[19] B. P. A. Kumar, E. T. Subramanium, K. M. Jayan, S. Mukherjee, and R. K. Bhowmik, *Proceedings on the Symposium on Advances in Nuclear and Allied Instruments, India 1997* (Tata McGraw-Hill, New Delhi), pp. 51–55.
[20] D. C. Radford, Nucl. Instrum. Methods Phys. Res. A **361**, 297 (1995).
[21] D. C. Radford, http://radware.phy.ornl.gov/.
[22] N. S. Pattabiraman, S. N. Chintalapudi, and S. S. Ghugre, Nucl. Instrum. Methods Phys. Res. A **526**, 432 (2004).
[23] N. S. Pattabiraman, S. N. Chintalapudi, and S. S. Ghugre, Nucl. Instrum. Methods Phys. Res. A **526**, 439 (2004).
[24] N. S. Pattabiraman, S. S. Ghugre, S. K. Basu, U. Garg, S. Ray, A. K. Sinha, and S. Zhu, Nucl. Instrum. Methods Phys. Res. A **562**, 222 (2006).
[25] M. Saha Sarkar *et al.*, Nucl. Instrum. Methods Phys. Res. A **491**, 113 (2002).
[26] M. Saha Sarkar *et al.*, Nucl. Instrum. Methods Phys. Res. A **556**, 266 (2006).
[27] G. Duchêne, F. A. Beck, P. J. Twin, G. de France, D. Curien, L. Han, C. W. Beausang, M. A. Bentley, P. J. Nolan, and J. Simpson, Nucl. Instrum. Methods Phys. Res. A **432**, 90 (1999).
[28] Z. Elekes, T. Belgya, G. L. Molnár, Á. Z. Kiss, M. Csatlós, J. Gulyás, A. Krasznahorkay, and Z. Máte, Nucl. Instrum. Methods Phys. Res. A **503**, 580 (2003).
[29] "NNDC Online Data Service," http://www.nndc.bnl.gov.
[30] K. S. Krane, R. M. Steffen, and R. M. Wheeler, Nucl. Data Tables **11**, 351 (1973).
[31] A. Krämer-Flecken, T. Morek, R. M. Lieder, G. H. W. Gast, H. M. Jäger, and W. Urban, Nucl. Instrum. Methods Phys. Res. A **275**, 333 (1989).
[32] F. S. Stephens, M. A. Deleplanque, R. M. Diamond, and A. O. Macchiavelli, Phys. Rev. Lett. **54**, 2584 (1985).
[33] J. C. Wells and N. Johnson, http://arxiv.org/abs/, Oak Ridge National Laboratory Report No. ORNL-6689, p. 44 (1991).
[34] E. S. Macias, W. D. Ruther, D. C. Camp, and R. G. Lanier, Comput. Phys. Commun. **11**, 75 (1976).
[35] R. J. Rouse Jr., G. L. Struble, R. G. Lanier, L. G. Mann, and E. S. Macias, Comput. Phys. Commun. **15**, 107 (1978).
[36] K. Starosta *et al.*, Nucl. Instrum. Methods Phys. Res. A **423**, 16 (1999).
[37] P. M. Jones, L. Wei, F. A. Beck, P. A. Butler, T. Byrski, G. Duchêne, G. de France, F. Hannachi, G. D. Jones, and B. Kharraja, Nucl. Instrum. Methods Phys. Res. A **362**, 556 (1995).
[38] T. Otsuka, M. Honma, T. Mizusaki, N. Shimizu, and Y. Utsuno, Prog. Part. Nucl. Phys. **47**, 319 (2001).
[39] A. N. Deacon *et al.*, Phys. Rev. C **82**, 034305 (2010).
[40] V. Tripathi *et al.*, Phys. Rev. C **73**, 054303 (2006).
[41] V. Tripathi *et al.*, Eur. Phys. J. A **25**, 101 (2005).
[42] V. Tripathi *et al.*, Phys. Rev. Lett. **94**, 162501 (2005).
[43] V. Tripathi *et al.*, Phys. Rev. C **76**, 021301(R) (2007).
[44] M. Kowalska, D. T. Yordanov, K. Blaum, P. Himpe, P. Lievens, S. Mallion, R. Neugart, G. Neyens, and N. Vermeulen, Phys. Rev. C **77**, 034307 (2008).
[45] M. Ionescu-Bujor *et al.*, Phys. Rev. C **73**, 024310 (2006).
[46] M. Wiedeking *et al.*, Phys. Rev. C **78**, 037302 (2008).
[47] D. Morris and A. Volya (2008), http://www.volya.net.
[48] E. K. Warburton and B. A. Brown, Phys. Rev. C **46**, 923 (1992).
[49] E. K. Warburton, J. A. Becker, and B. A. Brown, Phys. Rev. C **41**, 1147 (1990).
[50] J. B. Mcgrory, Phys. Rev. C **8**, 693 (1973).
[51] B. A. Brown, http://www.nscl.msu.edu/∼brown/resources/usd-05ajpg/p_32.jpg.